MJFAS
Malaysian Journal of Fundamental and Applied Sciences

Jamrus *et al.* | Malaysian Journal of Fundamental and Applied Sciences, Vol. 20 (2024) 528-543

RESEARCH ARTICLE

Stability Scrutinization of Time Depending Flow of a Ternary Hybrid Nanofluid Past a Shrinking Sheet with Wall Mass Suction Effect

Farah Nadzirah Jamrus[a,b]*, Anuar Ishak[a], Iskandar Waini[c]

[a]Department of Mathematical Sciences, Faculty of Science and Technology, Universiti Kebangsaan Malaysia, 43600 UKM Bangi, Selangor, Malaysia; [b]College of Computing, Informatics, and Mathematics, Universiti Teknologi MARA Cawangan Melaka Kampus Jasin, 77300, Merlimau, Melaka, Malaysia; [c]Fakulti Teknologi dan Kejuruteraan Industri dan Pembuatan, Universiti Teknikal Malaysia Melaka, Hang Tuah Jaya, 76100 Durian Tunggal, Melaka, Malaysia

Abstract The dynamics of unsteady flow of a ternary hybrid nanofluid on a stretching/shrinking sheet with wall mass suction is numerically analysed. In this study, a mixture of Al_2O_3, Cu, and TiO_2 is employed as additives in water, which serves as the base fluid. The equations governed the problem are simplified into a collection of ODEs by adopting the similarity transformation. Maintaining the flow on a shrinking sheet is reliant on the essential aspect of suction. Furthermore, augmenting the strength of suction amplifies the thermal conductivity process of the flow. Additionally, this study unveils dual solutions existing within a defined range of parameters. It has been determined that one solution exhibits long-term stability, whereas the other solution is deemed unstable through the stability analysis conducted.

Keywords: Nanofluid, heat transfer, dual solutions, stability analysis.

Introduction

Nowadays, a newly introduced fluid type referred to as nanofluids has replaced the usage of common liquid like water, ethylene glycol or oil in many industrial applications such as heating or cooling processes, power generation or chemical reactions. This new nanofluid was created by Choi *et al*. [1] and this fluid exhibits better thermal properties and enhanced heat transfer rates [2-4]. Nanofluids consist of one type of nanoparticle ranging in size from 1 to 100 nanometres that dispersed in the base fluid. Later, researchers shifted their attention towards hybrid nanofluid, which is an extended version of the nanofluids that comprised of a base fluid blended with two types of nanoparticles variants. These nanofluids have demonstrated commendable thermal conductivity characteristics and their heat transfer rate is boosted compared to single nanofluids. Hayat and Nadeem [5] conducted a heat transfer study on single and hybrid nanofluid, and they discovered the heat transfer of hybrid nanofluid were superior to those of CuO/water nanofluid.

However, the need for fluids with enhanced thermal conductivity and heat transmission rates has driven scientists to create a new fluid concept. Due to this, a new extension of nanofluid where three different types of nanoparticles are mixed in a stable manner within a base fluid has been introduced. This particular nanofluid is referred to as ternary hybrid nanofluids are believed possible to enhance thermal conductivity and can augment heat transfer rate. This new nanofluids recently has garnered the attention of researchers who are actively investigating their application in practical heat transfer scenarios. For example, Ramadhan *et al*. [6] observed ternary hybrid nanofluid that contains alumina (Al_2O_3), titania (TiO_2), and silica (SiO_2) in ethylene glycol reached optimal thermal conductivity when the volume concentration is 0.3% compared to 0.05%-0.2%. Moreover, Sundar *et al*. [7] synthesized a ternary hybrid nanofluid by dispersing iron oxide (Fe_3O_4), graphene oxide (GO) and titania (TiO_2) in ethylene glycol and

***For correspondence:**
fnadzirah@uitm.edu.my

Received: 15 Dec. 2023
Accepted: 14 April 2024

reported 14.32% increase in thermal efficiency. Dezfulizadeh *et al*. [8] conducted an analysis on the viscous dynamicity and thermal diffusivity of a ternary hybrid nanofluid Cu-SiO_2-MWCNT/water. They also developed practical correlations in this context. Ahmed *et al*. [9] reported on the impact of ZnO-Al_2O_3-TiO_2/distilled water on the heat transfer in a square flow conduit. Following, the rates of heat transfer for GO-TiO_2-Ag/water and rGO-TiO_2-Ag/water composites are significantly higher compared to those of water, as demonstrated by Mohammed Zayan *et al*. [10]. Elnaqeeb *et al*. [11] examined ternary hybrid nanofluid flow behaviour in a closed rectangular domain, where nanoparticles of different shapes and lower densities are suspended in water. The study focused on understanding the dynamics of these nanoparticles as they are carried by the water within the boundary layer. Flow of TiO_2-$CoFe_2O_4$-MgO/water with magnetic effect over a moving cylinder was investigated by Alharbi *et al*. [12] using computational parametric continuation approach. In the meantime, Madhukesh *et al*. [13] directed their attention towards examining how the thermal performance of a flow of Al_2O_3-Cu-TiO_2/water within an inclined cylinder/plate is influenced by factors such as inclined geometry, porosity, and the presence of heat source/sink. Thermal performance of rotating flow of Al_2O_3-SiC-MWCNT/water with radiation and fluid dissipation due to viscosity was examined by Sarangi *et al*. [14]. Animasaun *et al*. [15] explored the effect of magnetic flux density and heat source/sink on the flow of Ag-Al_2O_3-Al/water at the stagnation point over a sheet being convectively heated. The stagnation point flow of Cu-Al_2O_3-TiO_2/water over a heated stretching/shrinking sheet with heat generation/absorption and velocity slip effects was investigated by Mahmood *et al*. [16]. Later, Mahmood *et al*. [17] investigated the flow of Cu-Fe_2O_4-SiO_2/water at the stagnation point around a heated stretching/shrinking cylinder while being influenced by both suction and a heat source.

Flow within boundary layer is a prevalent occurrence in engineering and industrial manufacturing processes like polymer sheet manipulation, rolling at elevated temperatures, and manufacturing glass fibre and paper [18]. These flow phenomena frequently occur on surfaces experiencing stretching or shrinking. Sakiadis [19] introduced the concept of boundary layer flow on a moving surface, establishing his pioneering role in this field. Later, Crane [20] utilized this concept to study two-dimensional steady flow on a stretched surface in a viscous fluid. However, the investigation of shrinking surface has been less emphasized compared to surface stretching. Goldstein [21] found that fluid flow on a shrinking surface move in a rearward direction, distinguishing it from flow on a stretched surface. Meanwhile, Miklavčič and Wang [22] revealed that suction effect is essential for the fluid flow sustainability across a shrinking sheet. Halima *et al*. [23] noted that Ludwig Prandtl used injection/suction to delay boundary layer separation. Several causes exist for delaying boundary layer separation, including flow instability. Delaying separation improves flow stability and control and manoeuvrability. Heat transport is also reduced in stationary zones caused by boundary layer separation. By delaying separation, the boundary layer stays linked longer throughout the surface, improving heat transfer. As opposed to that, many studies conducted are about scrutinizing the steady fluid flow past a shrinking sheet, but less attention is paid to the time dependent flow. The comprehension of unsteady flow holds significant importance in disciplines such as fluid mechanics and aerodynamics since it enables engineers and scientists to anticipate and manipulate the dynamics of fluids inside various systems. The design and analysis of various systems, including aircraft, autos, pipelines, and environmental processes, are heavily influenced by its substantial function [24]. Unlike steady flows, unsteady flows behave differently. The boundary layer separation is increased because of a time-dependent factor in the mathematical models [25-26]. Consequently, extensive research has been conducted on the phenomenon of unsteady flow over a shrinking sheet with the presence of suction effect. A literature search on this particular flow revealed only a limited number of publications, as it represents a relatively novel type of flow. Unsteady flow over a shrinking sheet with mass transfer was pioneered by Fang *et al*. [27], who uncovered the presence of several solutions in a defined interval of mass suction and unsteadiness parameters. Subsequently, Rohni *et al*. [28] scrutinized the identical issue explored in [27], but in the context of nanofluids while Reddy *et al*. [29] analysed a comparable issue as discussed in [27], but they focused on hybrid nanofluid and took into account slip effects. The manufacturing processes of extrusion and rolling necessitate the shrinking of materials, a phenomenon also prevalent in polymer engineering for shaping and processing polymers to attain specific qualities. In metallurgy, shrinking operations are integral to metal heat treatment and forming. As a result, researchers are increasingly emphasizing the practical importance of exploring surfaces undergoing shrinking in fluid dynamics and heat transfer analyses, considering various types of fluid, and investigating the effects of different parameters, as detailed in references [30-31]. These findings offer valuable insights for understanding and optimizing operations across diverse sectors.

Most boundary value problems involve non-linear equations that allow multiple solutions, which can be a valuable feature in scientific research and engineering design. Researchers frequently investigate these multiple solutions in order to enhance their comprehension of the problem or to identify solutions that align with particular criteria or constraints. They employ suitable methods, including stability analysis

as performed by Merkin [32], to thoroughly examine and describe these solutions. In research led by Merkin [32], an examination was carried out involving unsteady flow with mixed convection occurring within a porous medium. The findings of this investigation reveal the stability of the first solution and the instability of the second solution. Weidman *et al*. [33] led a similar analysis to assess the solution's stability across several values of the transpiration parameter. The findings are the same as the previous work done. Moreover, researchers have identified the existence of dual or multiple solutions arising from flow problems across a shrinking sheet. They have subsequently executed an identical analysis to validate the stability and physically realizable solution, such as Ishak [34], Lund *et al*. [35], Yahaya *et al*. [36], Waini *et al*. [37], Khashi'ie *et al*. [38], and Rasool *et al*. [39].

The literature review above emphasizes the significance and practicality of unsteady flow across a permeable shrinking sheet. Therefore, this study is conducted to scrutinize the boundary layer separation and heat transmission properties of unsteady flow over a permeable shrinking sheet while accounting for wall mass suction and concentrating on ternary hybrid nanofluid (Al_2O_3-Cu-TiO_2/water). We believe this work is new and has the potential to help other scientists learn a lot about how heat moves through ternary hybrid nanofluid and find the control factors that can postpone the distancing of the boundary layer and improve fluid dynamics and heat transfer. Ternary hybrid nanofluid formation involves disseminating Al_2O_3 and Cu into water and after that TiO_2 with different volume fractions. Xuan *et al*. [40] experimentally demonstrated that this particular type of ternary hybrid nanofluid possesses favourable thermal properties exhibiting effective heat transfer. Besides, it is predictable that in a defined interval, dual solutions are present for the suction, the unsteadiness, the shrinking and the volume fractions parameters. Accordingly, an assessment of solution steadiness is executed to verify the solutions' ability to remain unchanged or resist disturbances over time which has a practical and physical applications in various real-world scenarios.

Problem Formulation

A two-dimensional unsteady flow with wall mass suction over a shrinking sheet of ternary hybrid nanofluid is considered (see Figure 1).

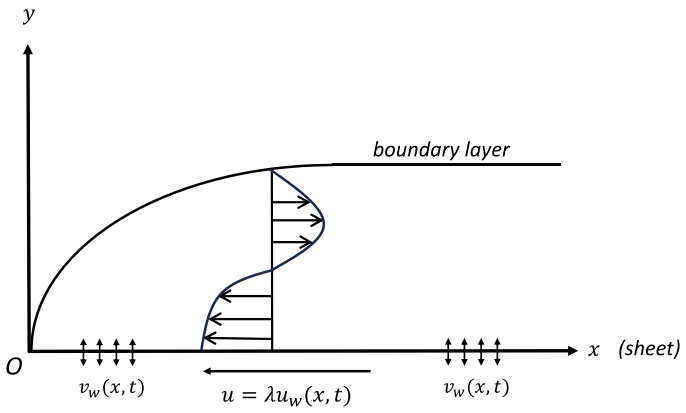

Figure 1. The problem geometric configuration

The ternary hybrid nanofluid is formed through the dispersion of Al_2O_3, Cu, and TiO_2 nanoparticles within a water medium and it is expected that fluid exhibits incompressibility and laminar flow. The wall mass suction velocity is assumed to be $v_w(x,t)$ and the shrinking velocity is $u_w(x,t) = cx/(1-\alpha t)$, where c is a positive constant, t is time, and α is the unsteadiness parameter of this problem. Consequently, the equations modelled for this problem are as follows [27-28], [37]:

$$\frac{\partial u}{\partial x} + \frac{\partial v}{\partial y} = 0, \tag{1}$$

$$\frac{\partial u}{\partial t} + u\frac{\partial u}{\partial x} + v\frac{\partial u}{\partial y} = \frac{\mu_{thnf}}{\rho_{thnf}}\frac{\partial^2 u}{\partial y^2}, \tag{2}$$

$$\frac{\partial T}{\partial t} + u\frac{\partial T}{\partial x} + v\frac{\partial T}{\partial y} = \frac{k_{thnf}}{(\rho C_p)_{thnf}}\frac{\partial^2 T}{\partial y^2}, \tag{3}$$

subject to the conditions,

$u = 0, v = 0, T = T_\infty$ for any x, y, when $t < 0$;
$u = \lambda u_w(x,t), v = v_w(x,t), T = T_w$ at $y = 0$, when $t \geq 0$;
$u \to 0, T \to T_\infty$ as $y \to \infty$. (4)

The velocities are represented as u (x direction) and v (y directions). Additionally, the parameter λ is introduced to describe the stretching/shrinking behaviour on the surface. Specifically, when $\lambda < 0$, it indicates a shrinking sheet; when $\lambda = 0$, it represents a stationary surface; and when $\lambda > 0$, it implies a stretching surface.

The thermophysical properties of ternary hybrid nanofluid are provided in Tables 1 and 2. It is imperative to note that the subscripts *f, nf*, *hnf*, and *thnf* correspond to the base fluid, nanofluid, hybrid nanofluid, and ternary hybrid nanofluid, respectively. Furthermore, the nanoparticles utilized in this research study are denoted as Al_2O_3 (subscript n_1), Cu (subscript n_2), and TiO_2 (subscript n_3). The respective volume fractions of these nanoparticles are represented by φ_1, φ_2, and φ_3.

Table 1. The thermophysical properties of ternary hybrid nanofluid [17]

Property	Ternary hybrid nanofluid's correlations
Dynamic viscosity	$\mu_{thnf} = \frac{\mu_{nf}}{(1-\varphi_1)^{2.5}(1-\varphi_2)^{2.5}(1-\varphi_3)^{2.5}}$
Density	$\rho_{thnf} = (1-\varphi_3)\{(1-\varphi_2)[(1-\varphi_1)\rho_f + \varphi_1\rho_{n1}] + \varphi_2\rho_{n2}\} + \varphi_3\rho_{n3}$
Thermal conductivity	$\frac{k_{thnf}}{k_{hnf}} = \frac{k_{n3}+2k_{hnf}-2\varphi_3(k_{hnf}-k_{n3})}{k_{n3}+2k_{hnf}+\varphi_3(k_{hnf}-k_{n3})}$, where $\frac{k_{hnf}}{k_{nf}} = \frac{k_{n2}+2k_{nf}-2\varphi_2(k_{nf}-k_{n2})}{k_{n2}+2k_{nf}+\varphi_2(k_{nf}-k_{n2})}$, where $\frac{k_{nf}}{k_f} = \frac{k_{n1}+2k_f-2\varphi_1(k_f-k_{n1})}{k_{n1}+2k_f+\varphi_1(k_f-k_{n1})}$.
Heat capacity	$(\rho C_p)h_{thnf} = (1-\varphi_3)\{(1-\varphi_2)[(1-\varphi_1)(\rho C_p)_f + \varphi_1(\rho C_p)_{n1}] + \varphi_2(\rho C_p)_{n2}\} + \varphi_3(\rho C_p)_{n3}$

Table 2. Thermophysical properties with respect to nanoparticles as well as water [41]

Property	Al_2O_3	Cu	TiO_2	Water
$C_p(J/kgK)$	765	385	686.5	4179
$\rho(kg/m^3)$	3970	8933	4250	997.1
$k(W/mK)$	40	400	8.9538	0.613
Prandtl Number, Pr				6.2

By using the following set of dimensionless variables that introduced by Fang *et al*. [27],

$$\psi = x\sqrt{\frac{c\nu_f}{1-\alpha t}}f(\eta), \eta = y\sqrt{\frac{c}{\nu_f(1-\alpha t)}}, \theta = \frac{T-T_\infty}{T_w-T_\infty}, \tag{5}$$

Here, ψ represents the stream function that fulfils the condition stated in Eq. (1) and ν_f is the base fluid kinematic viscosity. By utilizing the definition for the velocity components $u = \partial\psi/\partial y$ and $v = -\partial\psi/\partial x$, the velocities can be stated as

$$u = \frac{cx}{1-\alpha t}f'(\eta) \text{ and } v = -\sqrt{\frac{c\nu_f}{1-\alpha t}}f(\eta). \tag{6}$$

The wall mass transfer velocity takes the form

$$v_w(x,t) = -\sqrt{\frac{c\nu_f}{1-\alpha t}}S, \tag{7}$$

where S is the wall mass transfer parameter. In this study, only the case $S > 0$ (suction) is considered. By substituting (5) and (6) into Eq. (1)-(3), the following ODEs are obtained:

$$\frac{\mu_{thnf}/\mu_f}{\rho_{thnf}/\rho_f}f''' + ff'' - f'^2 - \beta\left(f' + \frac{\eta}{2}f''\right) = 0, \tag{8}$$

$$\frac{1}{Pr}\frac{k_{thnf}/k_f}{(\rho C_p)_{thnf}/(\rho C_p)_f}\theta'' + f\theta' - \beta\frac{\eta}{2}\theta' = 0, \tag{9}$$

bound to the boundary conditions

$$f(0) = S, f'(0) = \lambda, \theta(0) = 1;$$
$$f'(\eta) \to 0, \theta(\eta) \to 0 \text{ as } \eta \to \infty. \tag{10}$$

$\beta = \alpha/c$ in Eq. (8) and (9) represents the unsteadiness parameter. In the context of this study, we are examining a decelerating shrinking sheet characterized by a parameter β that satisfies the condition $\beta \leq 0$.

The coefficient of skin friction C_f and the Nusselt number Nu_x, are expressed as

$$C_f = \frac{\tau_w}{\rho_f u_w^2} \text{ and } Nu_x = \frac{xq_w}{k_f(T_w-T_\infty)}, \tag{11}$$

with τ_w is the surface shear stress and q_w is the surface heat flux,

$$\tau_w = \mu_{thnf}\left(\frac{\partial u}{\partial y}\right)_{y=0} \text{ and } q_w = -k_{thnf}\left(\frac{\partial T}{\partial y}\right)_{y=0}. \tag{12}$$

By substituting (5) and (6) into (11) and using (12) yield

$$C_f Re_x^{1/2} = \frac{\mu_{thnf}}{\mu_f}f''(0) \text{ and } Nu_x Re_x^{-1/2} = -\frac{k_{thnf}}{k_f}\theta'(0), \tag{13}$$

where the local Reynolds number is $Re_x = u_w x/\nu_f = cx^2/\nu_f(1-\alpha t)$.

Stability Analysis

It is well-established that ordinary differential equations possess the property of admitting multiple solutions, commonly referred to as dual solutions, which encompass both the first and second solutions. These multiple solutions cannot be identified experimentally [42]. Therefore, mathematical analysis is used in multiple solution identification. Once the multiple solutions are identified, it is imperative to perform a stability test to ascertain the stability and instability of the respective solutions [32-33]. In stability analysis, the unsteady flow is considered where the flow state depends on time. This method aims to impose a perturbation on the time-independent flow and the stable solution is identified when it is time-varying solution with the smallest error.

The boundary value problem of Eq. (1)-(3) with the boundary conditions in (4) is considered to test the features of stability analysis. The new dimensionless variables time variable τ is introduced and use together with the variables in (5) and (6) to model the stability problem as $\tau \to \infty$, hence new similarity variables in term of η and τ are obtained:

$$u(x,t) = \frac{cx}{1-\alpha t}\frac{\partial f}{\partial \eta}(\eta,\tau), v(x,t) = -\sqrt{\frac{c\nu_f}{1-\alpha t}}f(\eta,\tau), \theta(\eta,\tau) = \frac{T-T_\infty}{T_w-T_\infty},$$
$$\eta = y\sqrt{\frac{c}{\nu_f(1-\alpha t)}}, \tau = \frac{ct}{1-\alpha t} \quad (14)$$

Using (14), Eq. (2) and (3) become

$$\frac{\mu_{thnf}/\mu_f}{\rho_{thnf}/\rho_f}\frac{\partial^3 f}{\partial \eta^3} + f\frac{\partial^2 f}{\partial \eta^2} - \left(\frac{\partial f}{\partial \eta}\right)^2 - \beta\left(\frac{\eta}{2}\frac{\partial^2 f}{\partial \eta^2} + \frac{\partial f}{\partial \eta}\right) - (1+\beta\tau)\frac{\partial^2 f}{\partial \eta \partial \tau} = 0, \quad (15)$$

$$\frac{1}{Pr}\frac{k_{thnf}/k_f}{(\rho C_p)_{thnf}/(\rho C_p)_f}\frac{\partial^2 \theta}{\partial \eta^2} + f\frac{\partial \theta}{\partial \eta} - \beta\frac{\eta}{2}\frac{\partial \theta}{\partial \eta} - (1+\beta\tau)\frac{\partial \theta}{\partial \tau} = 0, \quad (16)$$

and Eq. (4) become

$$f(0,\tau) = S, \frac{\partial f}{\partial \eta}(0,\tau) = \lambda, \theta(0,\tau) = 1;$$
$$\frac{\partial f}{\partial \eta}(\eta,\tau) \to 0, \theta(\eta,\tau) \to 0 \text{ as } \eta \to \infty. \quad (17)$$

Afterward, a slight perturbation in the growth rate is introduced, denoted as $f = f_0(\eta)$ and $\theta = \theta_0(\eta)$. This approach aims to assess the stability of the obtained solution by utilizing the following relations

$$f(\eta,\tau) = f_0(\eta) + e^{-\gamma\tau}E(\eta,\tau),$$
$$\theta(\eta,\tau) = \theta_0(\eta) + e^{-\gamma\tau}H(\eta,\tau). \quad (18)$$

γ is the unknown eigenvalue, and function $E(\eta,\tau)$ and $H(\eta,\tau)$ are relatively small towards $f_0(\eta)$ and $\theta_0(\eta)$.

By using (18) and assumed that time approaching infinity ($\tau \to \infty$), then $e^{-\gamma t} \to 0$. Therefore, Eqs. (15) and (16) and boundary conditions (17) become

$$\frac{\mu_{thnf}/\mu_f}{\rho_{thnf}/\rho_f}\frac{\partial^3 E}{\partial \eta^3} + f_0\frac{\partial^2 E}{\partial \eta^2} + f_0''E - 2f_0'\frac{\partial E}{\partial \eta} - \beta\left(\frac{\eta}{2}\frac{\partial^2 E}{\partial \eta^2} + \frac{\partial E}{\partial \eta}\right)$$
$$+(1+\beta\tau)\left(\gamma\frac{\partial E}{\partial \eta} - \frac{\partial^2 E}{\partial \eta \partial \tau}\right) = 0, \quad (19)$$

$$\frac{1}{Pr}\frac{k_{thnf}/k_f}{(\rho C_p)_{thnf}/(\rho C_p)_f}\frac{\partial^2 H}{\partial \eta^2} + f_0\frac{\partial H}{\partial \eta} + \theta_0'E - \beta\frac{\eta}{2}\frac{\partial H}{\partial \eta} + (1+\beta\tau)\left(\gamma H - \frac{\partial H}{\partial \tau}\right) = 0, \quad (20)$$

subjected to:

$$E(0) = 0, E'(0) = 0, H(0) = 0;$$
$$E'(\eta) \to 0, H(\eta) \to 0 \text{ as } \eta \to \infty. \quad (21)$$

As proposed by Weidman *et al*. [33], when τ is set to zero in boundary value problem (19)-(21), leading to $E = E_0(\eta)$ and $H = H_0(\eta)$. Based on the given information, the following linear eigenvalue problem is obtained:

$$\frac{\mu_{thnf}/\mu_f}{\rho_{thnf}/\rho_f}E_0''' + f_0E_0'' + f_0''E_0 - 2f_0'E_0' - \beta\left(\frac{\eta}{2}E_0'' + E_0'\right) + \gamma E_0' = 0, \quad (22)$$

$$\frac{1}{Pr}\frac{k_{thnf}/k_f}{(\rho C_p)_{thnf}/(\rho C_p)_f}H_0'' + f_0H_0' + \theta'E_0 - \beta\frac{\eta}{2}H_0' + \gamma H_0 = 0, \quad (23)$$

subject to

$$E_0(0) = 0, E_0' = 0, H_0 = 0;$$
$$E_0'(\eta) \to 0, H_0(\eta) \to 0 \text{ as } \eta \to \infty. \quad (24)$$

By relaxing $E_0'(\eta) \to 0$ and instead, setting with $E_0''(0) = 1$, the eigenvalue problem is tackled. Therefore, new boundary conditions for (22) and (23) are

$$E_0(0) = 0, E_0' = 0, E_0''(0) = 1, H_0 = 0;$$
$$H_0(\eta) = 0 \text{ as } \eta \to \infty. \quad (25)$$

Upon solving the eigenvalue problem, an infinite number of eigenvalues will be obtained. A negative eigenvalue indicates the initial growth of disturbance, illustrating an unstable flow over time. On the other hand, a stable flow represented by a positive eigenvalue signifies the initial decay of disturbance as time progresses.

Results and Discussion

Utilizing the boundary value problem solver (bvp4c) in MATLAB software, we actively solved the governing equations Eqs. (8) and (9) with the specified boundary conditions (10). The bvp4c solver is a numerical solver commonly used in mathematics and engineering to solve boundary value problems (BVPs) connected to ordinary differential equations. This numerical solver was programmed with a finite difference that employs Lobatto IIIa scheme (three-stage) with fourth order accuracy. In this work, obtaining dual solutions, denoted as upper solutions and lower solutions, requires the provision of distinct initial guesses. The selection of these initial guesses follows a trial-and-error approach, with iterative refinement in cases where solver convergence is not achieved. To achieve both upper and lower solutions, a boundary layer thickness η_∞ is set to 15. Meanwhile, the tolerance limit in the bvp4c refers to the maximum allowable error between the computational and the actual solutions of the BVPs. This tolerance is applied to manage the precision of the solver and to ascertain when the solver has reached a satisfactory convergence to a solution. The tolerance limit used in this work is 10^{-10}. Furthermore, this study briefly examines the impact of various parameters, including suction, unsteadiness parameters, and the volumetric concentration of nanoparticles, on reduced skin friction coefficient, local Nusselt number, and fluid flow profiles. The analysis also encompasses the stability of the solutions. Careful consideration is given to selecting suitable values for these parameters to maintain adherence to far-field boundary conditions. This choice is determined by essential references and involves a trial-and-error method, considering the presence of dual solutions.

A comparison with the findings from previous research under various fluid models is used to verify the numerical solutions obtained, as presented in Table 3-6. Table 3 presents a comparative analysis of $-\theta(0)$ for regular fluid, as reported by Wang [43], Gorla and Sidawi [44], Waini *et al*. [37], Priyadharshini *et al*. [45] and the current study. The table includes values obtained for different Prandtl numbers. The current findings demonstrate a strong occurrence with the aforementioned studies. In the meantime, Table 4 depicts $f''(0)$ and $-\theta(0)$ values for Al_2O_3/water nanofluid where several values of φ_1 are considered, the present results show a close alignment with the findings from Waini *et al*. [46]. Meanwhile, for $\lambda = -1$, $f''(0)$ and $-\theta(0)$ values when Cu/water situation is considered for several values of β when $S = 2.1$ are shown in Table 5. These values are examined alongside the results from Waini *et al*. [37] and Roy *et al*. [47], demonstrating a strong concurrence. Variation of skin friction coefficients values for Cu-Al_2O_3/water when $\varphi_1 = 0.1, S = \beta = 0, \lambda = 1$ and $Pr = 6.135$ are given in Table 6 are align with the findings with those of Devi and Devi [48] and Rasool *et al*. [39]. As a consequence of Table 3-6, it is demonstrated the results attained in this study are reliable.

Table 3. $-\theta'(0)$ values for regular fluid $(\varphi_1 = \varphi_2 = \varphi_3 = 0)$ when $S = 0, \beta = 0, \lambda = 1$

Pr	Wang [43]	Gorla and Sidawi [44]	Waini *et al*. [37]	Priyadharshini *et al*. [45]	Present Results
2	0.9114	0.9114	0.911353	0.9113	0.91135
6.13	-	-	1.759682	-	1.75968
7	1.8954	1.8954	1.895400	1.8954	1.89540
20	3.3539	3.3539	3.353902	3.3539	3.35390

Table 4. $f''(0)$ and $-\theta'(0)$ values for Al_2O_3/water when $Pr = 6.2, S = \varphi_2 = \beta = 0, \lambda = 1$ (stretching sheet case)

φ_1	Waini *et al*. [46]		Present Results	
	$f''(0)$	$-\theta'(0)$	$f''(0)$	$-\theta'(0)$
0.05	-1.00538	1.62246	-1.00538	1.62246
0.10	-0.99877	1.49170	-0.99877	1.49170
0.15	-0.98184	1.37543	-0.98185	1.37542
0.20	-0.95592	1.27118	-0.95593	1.27117

Table 5. $f''(0)$ and $-\theta'(0)$ values for Cu/water when $\varphi_2 = 0.2, Pr = 6.2, S = 2.1$, and $\lambda = -1$ (shrinking sheet case)

	Roy *et al*. [47]				Present Results			
	$f''(0)$		$-\theta(0)$		$f''(0)$		$-\theta(0)$	
β	First Solution	Second Solution	First Solution	Second Solution	First Solution	Second Solution	First Solution	Second Solution
0	2.52897	0.586653	6.822302	6.693027	2.52897	0.584729	6.822453	6.693105
-0.4	2.395885	-0.482181	6.927484	6.754874	2.395251	-0.473473	6.927417	6.75547
-1	2.196043	-1.51016	7.074014	6.883723	2.194247	-1.491281	7.07368	6.884548
-5	0.858074	-6.516724	7.859843	7.656443	0.844435	-6.431507	7.858446	7.657801
-9	-0.487461	-10.743148	8.475325	8.276127	-0.517287	-10.58983	8.473316	8.277676

Table 6. Comparison values of $Re^{1/2}C_f$ for Cu-Al2O3/water when $Pr = 6.135, S = \beta = 0, \lambda = 1$ and $\varphi_1 = 0.1$

φ_2	$Re^{1/2}C_f$		
	Devi and Devi [48]	Rasool *et al*. [39]	Present Results
0.005	-1.327310	-1.325862	-1.327086
0.02	-1.409683	-1.404648	-1.409471
0.04	-1.520894	-1.511257	-1.520693
0.06	-1.634279	-1.620177	-1.634082

Effects of Physical Parameters on Physical Quantities of Interest

As stated previously, this paper assumes a decelerating shrinking sheet with $\beta \leq 0$. From Figures 2-7, the dual solutions happen when $\beta > \beta_c$, β_c is the bifurcation point where transition occurs between the first and second solutions. The results are aligned with the findings reported by Fang *et al*. [27], which indicate that there is no anticipated solution for $\beta \to -\infty$. Figure 2 demonstrates the variations of $Re_x^{1/2}C_f$ when $\lambda = -1$ and $\varphi_1 = \varphi_2 = \varphi_3 = 0.1$ for various values of S. The critical values β_c for $S = 2.0, 2.10, 2.15$ and 2.2 are $-0.3494, -3.1802, -7.0368$ and -15.4126, respectively. It is evident that as S increases, the points of β_c shift to the left and become smaller. Hence, it can be deduced that the boundary layer separation can be delayed by increasing the value of S. The increase in S also led to a rise in $Re_x^{1/2}C_f$ because suction on the shrinking sheet causes the fluid to approach the sheet more closely. As a result, the momentum boundary layer decreases in thickness (refer to Figure 8). Theoretically, the thinning of the boundary layer results in higher surface shear stress, thereby increasing the skin friction coefficient. In addition, increasing S also lead to the increasing value of $Re_x^{-1/2}Nu_x$ for both solutions as demonstrated in Figure 3. Suction draws fluid towards the shrinking plate, reducing thermal boundary layer thickness. The augmented heat transfer from the sheet to the fluid, facilitated by the thinner thermal boundary layer, is reflected in Figure 9.

Meanwhile, in Figure 4, as φ_3 decreases, the critical values β_c also decrease where the critical values for $\varphi_3 = 0.05$ and 0.1 are -13.5924 and -3.1802, respectively. Based on Figure 4, it can be assumed that β_c for $\varphi_3 = 0.005$ will go further to the bottom left. It follows that a decrease in the value of φ_3 will result in a postponement of the boundary layer's separation. Additionally, the skin friction coefficient for the first solution decreases while for the second solution increases because of φ_3 increasing. An increase in the volume fraction results in an elevation of the fluid's viscosity. The heightened viscosity leads to more resistance to the movement of fluid, resulting in a decrease in fluid velocity (refer to Figure 16). In practical terms, a reduction in fluid velocity indicates lower surface shear stress and a subsequently

decreased skin friction coefficient. Meanwhile, with the rise of φ_3, Figure 5 shows the decreases in $Re_x^{-1/2}Nu_x$ for both solutions. On account of the rising nanoparticle volume fraction, the fluid will become more viscous and cause resistance to the fluid flow. Consequently, the fluid's ability to transfer heat through convection decreases, leading to a direct decrease in the local Nusselt number.

The variations of $Re_x^{1/2}C_f$ and $Re_x^{-1/2}Nu_x$ with β for different type of nanofluids: single nanofluid, hybrid nanofluid, and ternary hybrid nanofluid are presented in Figures 6 and 7. These variations are shown when the parameters $\lambda = -1, S = 2.1$, and $Pr = 6.2$. According to the graph presented in Fig. 6, critical value β_c for ternary hybrid nanofluid is smaller than critical value β_c for single nanofluid, which are -3.1802 and -1.5785, respectively. In contrast, the critical value β_c for the hybrid nanofluid case is anticipated to exhibit a downward shift towards the lower left region of the graph. Additionally, it also can be noted from Figures 6 and 7 that ternary hybrid nanofluid possesses moderate values of $Re_x^{1/2}C_f$ and $Re_x^{-1/2}Nu_x$ for both solutions, in contradistinction to the hybrid nanofluid and single nanofluid. As indicated by Mahmood *et al*. [17] and Manjunatha *et al*. [41], ternary hybrid nanofluid exhibits enhanced heat transfer compared to both nanofluid and hybrid nanofluid. However, the inclusion of suction, unsteady conditions, and shrinking parameters in this study may yield contrary results.

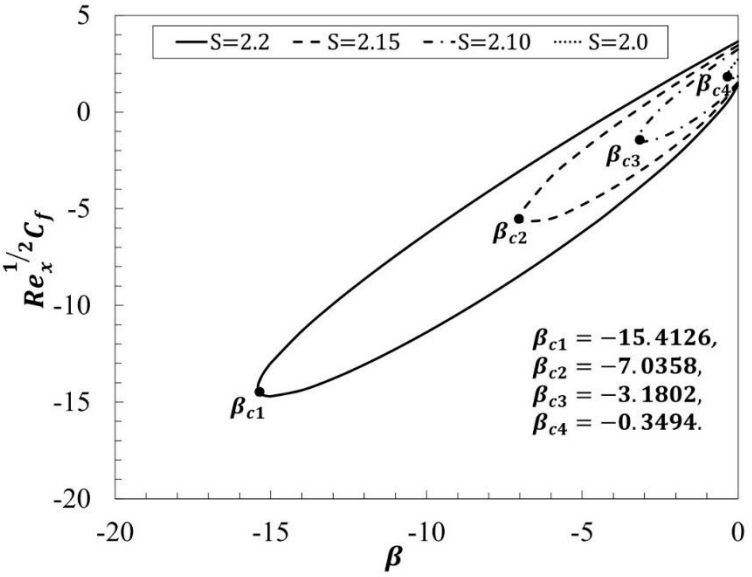

Figure 2. Variations of $Re_x^{1/2}C_f$ with respect to β for various value of S

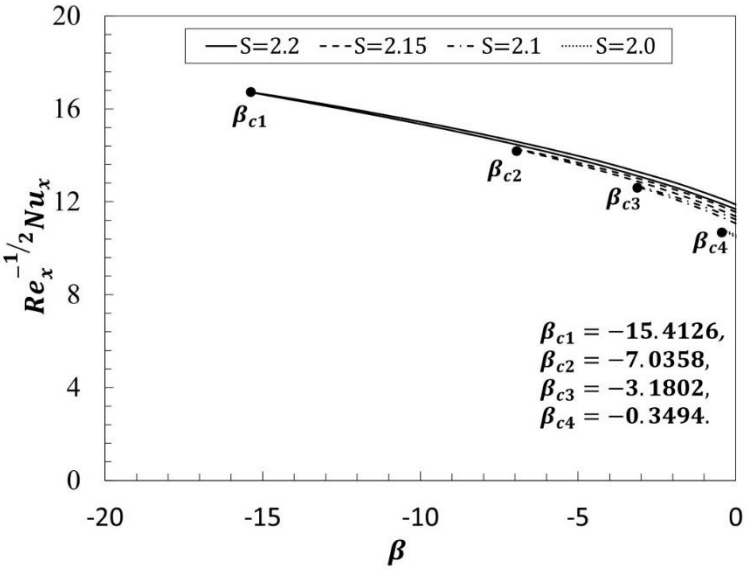

Figure 3. Variations of $Re_x^{1/2}Nu_x$ with respect to β for various value of S

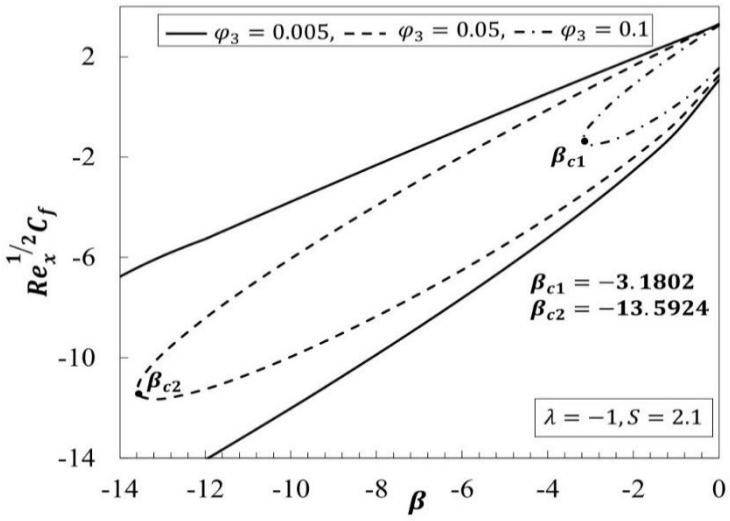

Figure 4. Variations of $Re_x^{1/2} C_f$ with respect to β for various value of φ_3

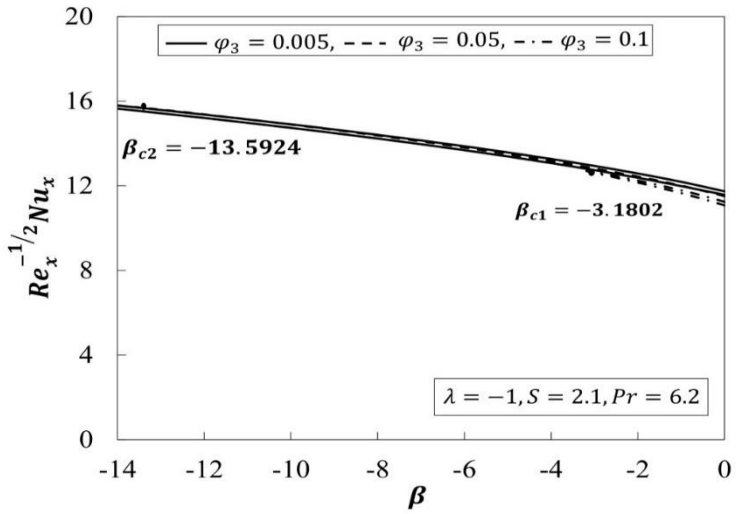

Figure 5. Variations of $Re_x^{1/2} Nu_x$ with respect to β for various value of φ_3

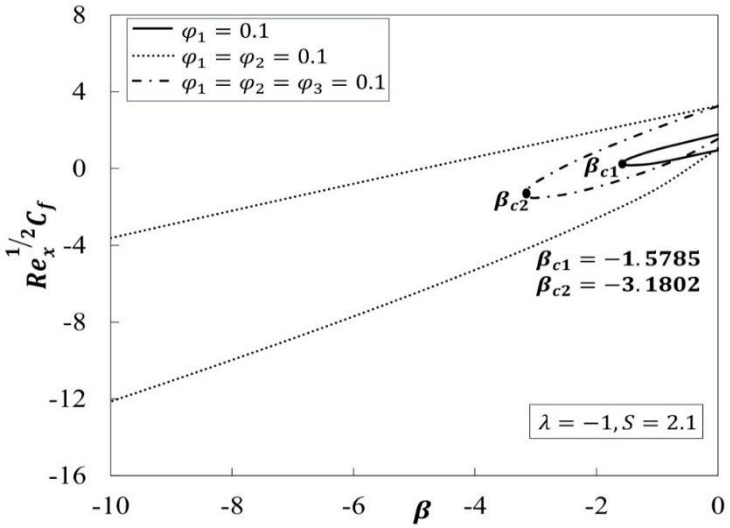

Figure 6. Comparison of $Re_x^{1/2} C_f$ variations between nanofluid, hybrid nanofluid and ternary nanofluid

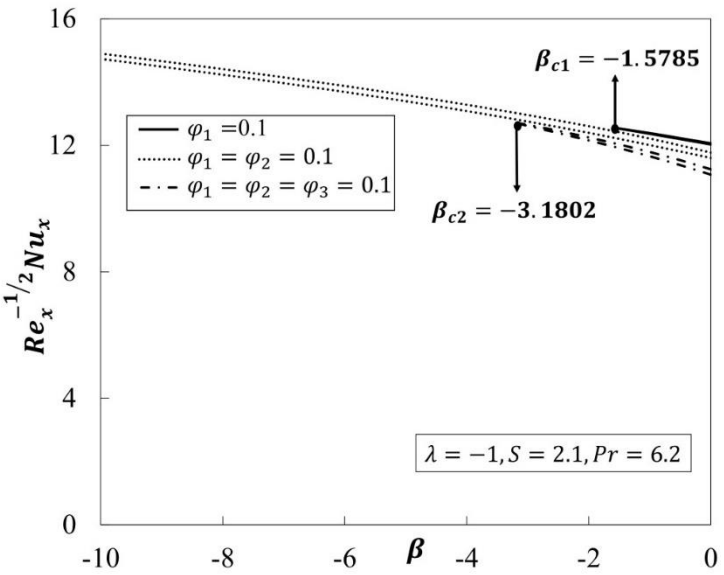

Figure 7. Comparison of $Re_x^{-1/2}Nu_x$ variations between nanofluid, hybrid nanofluid and ternary nanofluid

Effects of Physical Parameters on Fluid Profiles

As suction intensifies, Figure 8 illustrates a declining trend in the thickness of the momentum boundary layer and consequently the velocity gradients exhibit an upward trend on the shrinking sheet, thus the skin friction coefficient in Figure 2 increases. Furthermore, Figure 8 exhibits dimensionless velocity profiles for different values of S, indicating the presence of two distinct velocity profiles. As depicted in the diagram, the initial solution exhibits a direct correlation with the growth in S values. Similarly, when the suction value is increased, the thermal boundary layer is thinning cause the temperature gradient increases, hence the fluid temperature experiences a slight decrease for both solutions in Figure 9. Physically, the increased temperature gradients lead to the boosted convective heat transport, and consequently increased rate of heat transfer as seen in Figure 3.

Figures 10 and 11 illustrates the volume fraction impact ($\varphi_1 = \varphi_2 = 0.1, \varphi_3 = 0.005$,0.05, and 0.1) on $f'(\eta)$ and $\theta(\eta)$ when $\beta = -1, \lambda - 1, S = 2.1$ and $Pr = 6.2$. The finding in Figure 10 suggests that an increase in the volume fraction result in the thickening of the momentum boundary layer. Hence, the velocity gradients decrease correspond to the reduced flow velocity and diminishing rate of skin friction coefficient as depicted in Figure 4. Meanwhile, Figure 11 illustrates when the volume fraction is raised, it leads to the increment of thermal boundary layer thickness, consequently the temperature gradients decrease. When temperature gradients decrease, lower convective transport lead to the low rate of fluid heat transfer as depicted in Figure 5. Moreover, Figures 8-11 clearly demonstrate the asymptotic fulfilment of the far-field boundary criteria outlined in Eq. (10). As highlighted by Anuar [49], it is crucial for velocity and temperature profiles to conform to the designated boundary conditions, guaranteeing the precision and reliability of the numerical results.

Figure 12 illustrates the eigenvalues variations for values of β when $\lambda = -1, S = 2.1, \varphi_1 = \varphi_2 = 0.1, \varphi_3 = 0.05$ and $Pr = 6.2$. Notably, the critical point $\beta_c = -13.5924$ is the point that separates the first and second solution. The first solution is considered stable, as its smallest eigenvalue is positive, indicating that disturbances initiated at this point decay over time. On the other hand, the second solution can be characterized as unstable since its smallest eigenvalue is negative, suggesting the growth of disturbances starting from this point. Moreover, it is evident that the smallest eigenvalues for both solutions tend to approach zero as β approaches the critical point $\beta_c = -13.5924$. This observation indicates the occurrence of a flow transition from the stable to unstable phase at the critical point.

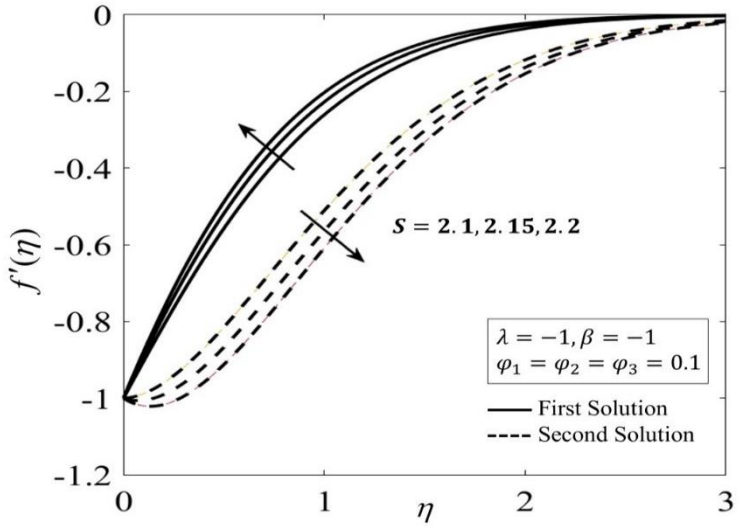

Figure 8. Velocity profile for different values of S

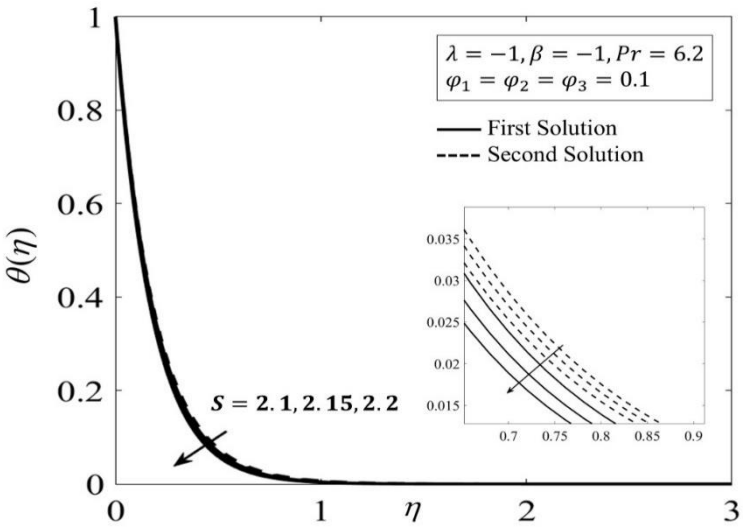

Figure 9. Temperature profile for different values of S

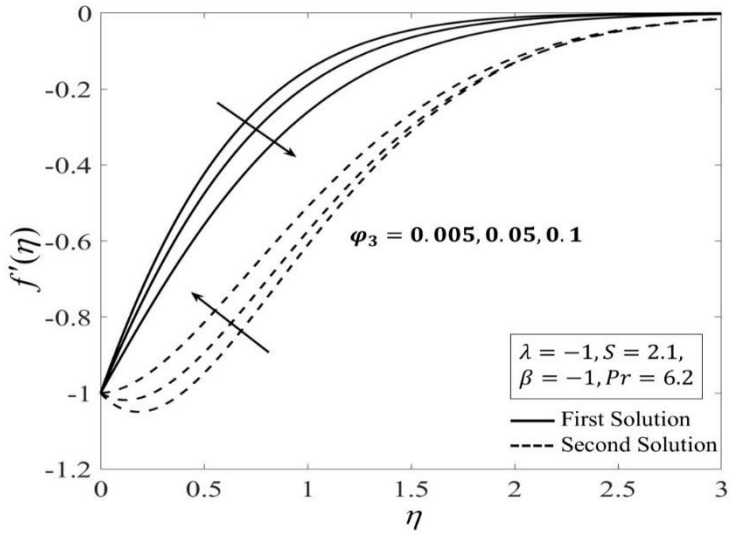

Figure 10. Velocity profile for various φ_3

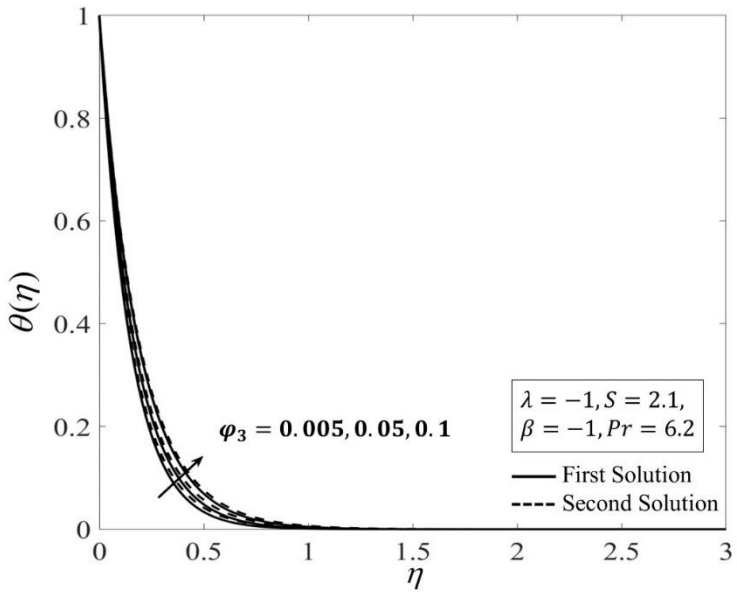

Figure 11. Temperature profile for various φ_3

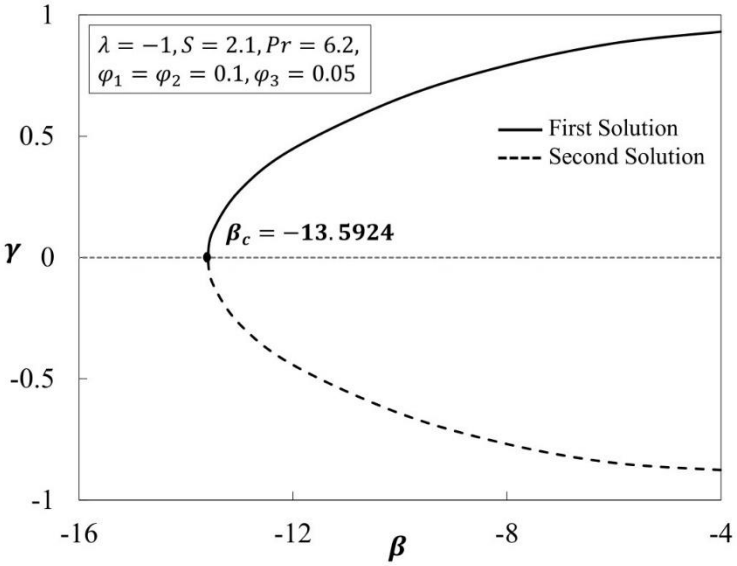

Figure 12. Variation of the eigenvalue γ with different values of β

Conclusions

The characteristics of an unsteady ternary hybrid nanofluid flow (composed of Al_2O_3-Cu-TiO_2 nanoparticles dispersed in water) across a shrinking sheet, considering the influence of mass suction is scrutinized. These findings' validity is established through a comparative analysis with prior research, which demonstrates a consistent alignment between the obtained results and those reported in previous studies. The impact of suction S, unsteadiness β, and volume fraction φ_3 parameters on the fluid motion and heat transmission are inspected. The result indicated that manipulating the suction parameter leads to an augmentation in fluid velocity for both solutions. It also noted that fluid temperature decreases for both solutions as the suction parameter increases. By increasing the strength of the suction parameter, it is observed that the boundary layer separation can be delayed. Conversely, a smaller value of φ_3 contributes to the postponement of boundary layer separation. For the increasing volume fraction φ_3, it is observed that $Re_x^{1/2} C_f$ decreases and $Re_x^{-1/2} Nu_x$ increases, as β decreases. In addition to this, the

stability of the first solution has been verified, whereas the second solution has been determined to be unstable by implementing the stability analysis.

Conflicts of Interest

The author(s) declare(s) that there is no conflict of interest regarding the publication of this paper.

Acknowledgment

A grateful acknowledgement goes to Universiti Kebangsaan Malaysia (DIP-2023-005), Universiti Teknologi MARA Cawangan Melaka, and Universiti Teknikal Malaysia Melaka.

References

[1] S. U. S. Choi and J. A. Eastman. (1995). Enhancing thermal conductivity of fluids with nanoparticles. *Proceedings of the 1995 ASME International Mechanical Engineering Congress and Exposition,* FED 231/MD *66*, 99-105.

[2] A. Gavili and T. Isfahani. (2020). Experimental investigation of transient heat transfer coefficient in natural convection with Al_2O_3-nanofluids. *Heat and Mass Transfer, 56*(3), 901-911. https://doi.org/10.1007/s00231-019-02752-5.

[3] R. Mohebbi and M. M. Rashidi. (2017). Numerical simulation of natural convection heat transfer of a nanofluid in an L-shaped enclosure with a heating obstacle. *J Taiwan Inst Chem Eng.*, *72*, 70-84. https://doi.org/10.1016/j.jtice.2017.01.006.

[4] M. Turkyilmazoglu. (2020). Single phase nanofluids in fluid mechanics and their hydrodynamic linear stability analysis. *Comput Methods Programs Biomed., 187*, 105171. https://doi.org/10.1016/j.cmpb.2019.105171.

[5] Hayat and S. Nadeem. (2017). Heat transfer enhancement with Ag-CuO/water hybrid nanofluid. *Results Phys., 7*, 2317-2324. https://doi.org/10.1016/j.rinp.2017.06.034.

[6] A. I. Ramadhan, W. H. Azmi, and R. Mamat. (2021). Experimental investigation of thermo-physical properties of tri-hybrid nanoparticles in water-ethylene glycol mixture. *Walailak Journal of Science and Technology (WJST), 18*(8). https://doi.org/10.48048/wjst.2021.9335.

[7] L. S. Sundar, K. V. V. Chandra Mouli, Z. Said, and A. C. M. Sousa. (2021). Heat transfer and second law analysis of ethylene glycol-based ternary hybrid nanofluid under laminar flow. *J Therm Sci Eng Appl.,* 13(5). https://doi.org/10.1115/1.4050228.

[8] A. Dezfulizadeh, A. Aghaei, A. H. Joshaghani, and M. M. Najafizadeh. (2021). An experimental study on dynamic viscosity and thermal conductivity of water-Cu-SiO_2-MWCNT ternary hybrid nanofluid and the development of practical correlations. *Powder Technol., 389*, 215-234. https://doi.org/10.1016/j.powtec.2021.05.029.

[9] W. Ahmed *et al*. (2021). Heat transfer growth of sonochemically synthesized novel mixed metal oxide ZnO+Al_2O_3+TiO_2/DW based ternary hybrid nanofluids in a square flow conduit. *Renewable and Sustainable Energy Reviews, 145*, 111025. https://doi.org/10.1016/j.rser.2021.111025.

[10] J. Mohammed Zayan *et al*. (2023). Synthesis and characterization of novel ternary-hybrid nanoparticles as thermal additives. *Materials, 16*(1). https://doi.org/10.3390/ma16010173.

[11] T. Elnaqeeb, I. L. Animasaun, and N. A. Shah. (2021). Ternary-hybrid nanofluids: significance of suction and dual-stretching on three-dimensional flow of water conveying nanoparticles with various shapes and densities. *Zeitschrift für Naturforschung A*, *76*(3), 231-243. https://doi.org/10.1515/zna-2020-0317.

[12] K. A. M. Alharbi *et al*. (2022). Computational valuation of darcy ternary-hybrid nanofluid flow across an extending cylinder with induction effects. *Micromachines (Basel), 13*(4), 588. https://doi.org/10.3390/mi13040588.

[13] J. K. Madhukesh, I. E. Sarris, B. C. Prasannakumara, and A. Abdulrahman. (2023). Investigation of thermal performance of ternary hybrid nanofluid flow in a permeable inclined cylinder/plate. *Energies (Basel), 16*(6), 2630. https://doi.org/10.3390/en16062630.

[14] M. K. Sarangi, D. N. Thatoi, M. K. Nayak, J. Prakash, K. Ramesh, and M. Azam. (2022). Rotational flow and thermal behavior of ternary hybrid nanomaterials at small and high Prandtl numbers. *International Communications in Heat and Mass Transfer*, *138*, 106337. https://doi.org/10.1016/j.icheatmasstransfer.2022.106337.

[15] I. L. Animasaun, S.-J. Yook, T. Muhammad, and A. Mathew. (2022). Dynamics of ternary-hybrid nanofluid subject to magnetic flux density and heat source or sink on a convectively heated surface. *Surfaces and Interfaces*, *28*, 101654. https://doi.org/10.1016/j.surfin.2021.101654.

[16] Z. Mahmood, Z. Iqbal, M. A. Alyami, B. Alqahtani, M. F. Yassen, and U. Khan. (2022). Influence of suction and heat source on MHD stagnation point flow of ternary hybrid nanofluid over convectively heated stretching/shrinking cylinder. *Advances in Mechanical Engineering, 14*(9), 168781322211262. https://doi.org/10.1177/16878132221126278.

[17] Z. Mahmood, N. A. Ahammad, S. E. Alhazmi, U. Khan, and M. Z. Bani-Fwaz. (2022). Ternary hybrid nanofluid near a stretching/ shrinking sheet with heat generation/ absorption and velocity slip on unsteady stagnation point flow. *Int J Mod Phys B, 36*(29). https://doi.org/10.1142/S0217979222502095.

[18] A. Mohammadi, M. H. Ahmadi, M. Bidi, F. Joda, A. Valero, and S. Uson. (2017). Exergy analysis of a combined

cooling, heating and power system integrated with wind turbine and compressed air energy storage system. *Energy Convers Manag*., *131*, 69-78. https://doi.org/10.1016/j.enconman.2016.11.003.
[19] B.C. Sakiadis. (1961). Boundary-layer behavior on continuous solid surfaces: I. Boundary-layer equations for two-dimensional and axisymmetric flow. *AIChE Journal*, *7*(1), 26-28. https://doi.org/10.1002/aic.690070108.
[20] L. J. Crane. (1970). Flow past a stretching plate. *Zeitschrift für angewandte Mathematik und Physik ZAMP, 21*(4), 645-647. https://doi.org/10.1007/BF01587695.
[21] S. Goldstein. (1965). On backward boundary layers and flow in converging passages. *J Fluid Mech., 21*(01), 33. https://doi.org/10.1017/S0022112065000034.
[22] M. Miklavčič and C. Wang. (2006). Viscous flow due to a shrinking sheet. *Q Appl Math, 64*(2), 283-290. Aprhttps://doi.org/10.1090/S0033-569X-06-01002-5.
[23] U. Halima, D. AM, and A. Sammani. (2023). Effects of injection/suction on unsteady mhd natural convective radiative flow of heat mass transfer in a plumb frequency. *Saudi Journal of Engineering and Technology*, *8*(07), 171-180. Julhttps://doi.org/10.36348/sjet.2023.v08i07.003.
[24] H. Chanson. (2004). Unsteady open channel flows: 2. Applications. *Hydraulics of Open Channel Flow*, 318-370. https://doi.org/10.1016/B978-075065978-9/50024-6.
[25] F. T. Smith. (1986). Steady and unsteady boundary-layer separation. *Annu Rev Fluid Mech.*, *18*(1), 197-220. https://doi.org/10.1146/annurev.fl.18.010186.001213.
[26] W. R. Sears and D. P. Telionis. (1975). Boundary-Layer Separation in Unsteady Flow. *SIAM J Appl Math*, *28*(1), 215-235. https://doi.org/10.1137/0128018.
[27] T. G. Fang, J. Zhang, and S.-S. Yao. (2009). Viscous flow over an unsteady shrinking sheet with mass transfer. *Chinese Physics Letters*, *26*(1), 014703. Janhttps://doi.org/10.1088/0256-307X/26/1/014703.
[28] A. M. Rohni, S. Ahmad, and I. Pop. (2012). Flow and heat transfer over an unsteady shrinking sheet with suction in nanofluids. *Int J Heat Mass Transf., 55*(7-8), 1888-1895. https://doi.org/10.1016/j.ijheatmasstransfer.2011.11.042.
[29] P. S. Reddy, P. Sreedevi, and A. J. Chamkha. (2023). Hybrid nanofluid heat and mass transfer characteristics over a stretching/shrinking sheet with slip effects. *Journal of Nanofluids, 12*(1), 251-260. https://doi.org/10.1166/jon.2023.1996.
[30] G. Murtaza, L. Bonik, E. Em. Tzirtzilakis, and M. Ferdows. (2023). Finite difference simulation on biomagnetic fluid flow and heat transfer with gold nanoparticles towards a shrinking sheet in the presence of a magnetic dipole. *IOCMA 2023, Basel Switzerland: MDPI.* 18. https://doi.org/10.3390/IOCMA2023-14398.
[31] R. I. Yahaya, N. Md Arifin, S. S. P. Mohamed Isa, and M. M. Rashidi. (2021). Magnetohydrodynamics boundary layer flow of micropolar fluid over an exponentially shrinking sheet with thermal radiation: Triple solutions and stability analysis. *Math Methods Appl Sci., 44*(13), 10578-10608. https://doi.org/10.1002/mma.7432.
[32] J. H. Merkin. (1986). On dual solutions occurring in mixed convection in a porous medium. *J Eng Math., 20*(2), 171-179. https://doi.org/10.1007/BF00042775.
[33] P. D. Weidman, D. G. Kubitschek, and A. M. J. Davis. (2006). The effect of transpiration on self-similar boundary layer flow over moving surfaces. *Int J Eng Sci., 44*(11-12), 730-737. https://doi.org/10.1016/j.ijengsci.2006.04.005.
[34] A. Ishak. (2014). Flow and heat transfer over a shrinking sheet: a stability analysis. I*nternational Journal of Mechanical, Aerospace, Industrial, Mechatronic and Manufacturing Engineering, 8*, 902-906. https://api.semanticscholar.org/CorpusID:30083030.
[35] L. A. Lund, Z. Omar, and I. Khan. (2019). Steady incompressible magnetohydrodynamics Casson boundary layer flow past a permeable vertical and exponentially shrinking sheet: A stability analysis. *Heat Transfer-Asian Research, 48*(8), 3538-3556. https://doi.org/10.1002/htj.21554.
[36] R. I. Yahaya, N. M. Arifin, R. Nazar, and I. Pop. (2020). Flow and heat transfer past a permeable stretching/shrinking sheet in Cu−Al_2O_3/water hybrid nanofluid. *Int J Numer Methods Heat Fluid Flow, 30*(3), 1197-1222. https://doi.org/10.1108/HFF-05-2019-0441.
[37] I. Waini, A. Ishak, and I. Pop. (2019). Unsteady flow and heat transfer past a stretching/shrinking sheet in a hybrid nanofluid. *Int J Heat Mass Transf., 136*, 288-297. https://doi.org/10.1016/j.ijheatmasstransfer.2019.02.101.
[38] N. Safwa Khashi'ie, N. C. Roșca, A. V. Roșca, and I. Pop. (2023). Dual solutions on MHD radiative three-dimensional bidirectional nanofluid flow over a non-linearly permeable shrinking sheet. *Alexandria Engineering Journal*, *71*, 401-411. https://doi.org/10.1016/j.aej.2023.03.066.
[39] G. Rasool, X. Wang, U. Yashkun, L. A. Lund, and H. Shahzad. (2023). Numerical treatment of hybrid water based nanofluid flow with effect of dissipation and Joule heating over a shrinking surface: Stability analysis. *J Magn Magn Mater., 571*, 170587. https://doi.org/10.1016/j.jmmm.2023.170587.
[40] Z. Xuan, Y. Zhai, M. Ma, Y. Li, and H. Wang. (2021). Thermo-economic performance and sensitivity analysis of ternary hybrid nanofluids. *J Mol Liq., 323*, 114889. https://doi.org/10.1016/j.molliq.2020.114889.
[41] S. Manjunatha, V. Puneeth, B. J. Gireesha, and A. J. Chamkha. (2022). Theoretical study of convective heat transfer in ternary nanofluid flowing past a stretching sheet. *Journal of Applied and Computational Mechanics, 8*(4), 1279-1286. https://doi.org/10.22055/jacm.2021.37698.3067.
[42] J. Raza. (2018). Similarity solutions of boundary layer flows in a channel filled by non-newtonian fluids. Universiti Utara Malaysia, Changlun, Malaysia.
[43] C. Y. Wang. (1989). Free convection on a vertical stretching surface. *ZAMM - Journal of Applied Mathematics and Mechanics / Zeitschrift für Angewandte Mathematik und Mechanik*, *69*(11), 418-420. https://doi.org/10.1002/zamm.19890691115.
[44] R. S. R. Gorla and I. Sidawi. (1994). Free convection on a vertical stretching surface with suction and blowing. *Applied Scientific Research*, *52*(3), 247-257. https://doi.org/10.1007/BF00853952.
[45] P. Priyadharshini, M. V. Archana, N. A. Shah, and M. H. Alshehri. (2023). ternary hybrid nanofluid flow emerging on a symmetrically stretching sheet optimization with machine learning prediction scheme. *Symmetry (Basel), 15*(6), 1225. https://doi.org/10.3390/sym15061225.

[46] Iskandar Waini, Farah Nadzirah Jamrus, Abdul Rahman Mohd Kasim, Anuar Ishak, and Ioan Pop. (2023). Homogeneous-heterogeneous reactions on Al_2O_3-Cu hybrid nanofluid flow over a shrinking sheet. *Journal of Advanced Research in Fluid Mechanics and Thermal Sciences*, *102*(1), 85-97. https://doi.org/10.37934/arfmts.102.1.8597.

[47] N. C. Roy, A. Hossain, and I. Pop. (2022). Flow and heat transfer of MHD dusty hybrid nanofluids over a shrinking sheet. *Chinese Journal of Physics*, *77*, 1342-1356. https://doi.org/10.1016/j.cjph.2021.12.012.

[48] S. S. U. Devi and S. P. A. Devi. (2017). Heat transfer enhancement of $Cu-Al_2O_3$/water hybrid nanofluid flow over a stretching sheet. *Journal of the Nigerian Mathematical Society,* *36*(2), 419-433. https://www.scopus.com/inward/record.uri?eid=2-s2.0 85056632790&partnerID=40&md5=a194e2bee97b97967acf94f36023af87.

[49] A. Ishak. (2010). Aliran lapisan sempadan bersebelahan plat tegak dengan suhu permukaan malar (boundary layer flow adjacent to a vertical plate with constant surface temperature). *Sains Malaysiana*, *39*(6),1035-1039.